Doppler shift on meteor scatter pings

Mike Hasselbeck, WB2FKO

mph@sportscliche.com

First draft: 12 October 2020; revised 7 July 2021

Abstract

A general model has been developed to calculate the Doppler shift on radio communication paths due to fast moving meteor heads. Both forward and backward meteor scattering are analyzed as well as frequency chirp that occurs over the duration of a ping. The key roles of head velocity vector, path geometry, and radio frequency are demonstrated. The frequency synchronization schemes of the FSK441 and MSK144 protocols are also examined. Depending on the operating conditions, these modes may not be able to compensate for very large Doppler shifts induced by the fast-moving head. This suggests that the majority of meteor scatter decodes are due to scattering from the relatively stationary trail.

Keywords: meteor scatter, FSK441, MSK144, Doppler

Introduction. A Doppler frequency shift occurs when the path between the emitter and receiver of a coherent wave changes as function of time. A path length decrease causes the frequency to increase or up-chirp, whereas an increasing separation distance results in down-chirp. If the separation distance remains constant, a relative velocity between transmitter and receiver will not produce a Doppler shift. For example, a receiver moving in a rapid circular orbit around a stationary emitter will not detect a Doppler shift because their separation is at a fixed radius.

Radio communication between distant stations is often possible by scattering from fast moving meteors disintegrating in the E-layer. Ionization produces a short-lived plasma that may reflect a radio wave depending on its wavelength [1]. There are two essential components of the ionization: i) the volume immediately surrounding the meteor head and ii) an extended trail. Compared to the head, the trail generally has lower ionization density, is longer-lived, and is relatively stationary. The presence of a large Doppler shift and subsequent chirp can be used to distinguish the head and trail in radio scattering experiments [2].

Of interest for amateur radio work is the behavior of the scattered wave as the operating frequency moves from VHF to UHF. The minimum ionization density needed for reflection goes as the square of the frequency, the amount of Doppler shift increases in direct proportion to the frequency, and reflected signals (pings) become shorter and less frequent.

Forward Scattering. Doppler frequency shifting of radio waves by meteors was first analyzed by Manning in 1948 using the Pythagorean theorem [3]. Referring to Figure 1, a meteor traveling at velocity v appears in the path between two stations. For short pings considered here, it is assumed that v is constant. Vector decomposition of v produces three components on the orthogonal axes in the reference frame of the stations: a longitudinal component v_x along the direct path between the stations, a transverse component v_y in the perpendicular horizontal direction, and a perpendicular vertical component v_z. The vertical component v_z represents the meteor's descent towards the earth's surface at a shallow angle. It is assumed to have negligible magnitude compared to the two velocity components in the surface plane. The angle α defines $v_x = v\cos\alpha$ and $v_y = v\sin\alpha$, which determines the relative contribution of the longitudinal and transverse components.

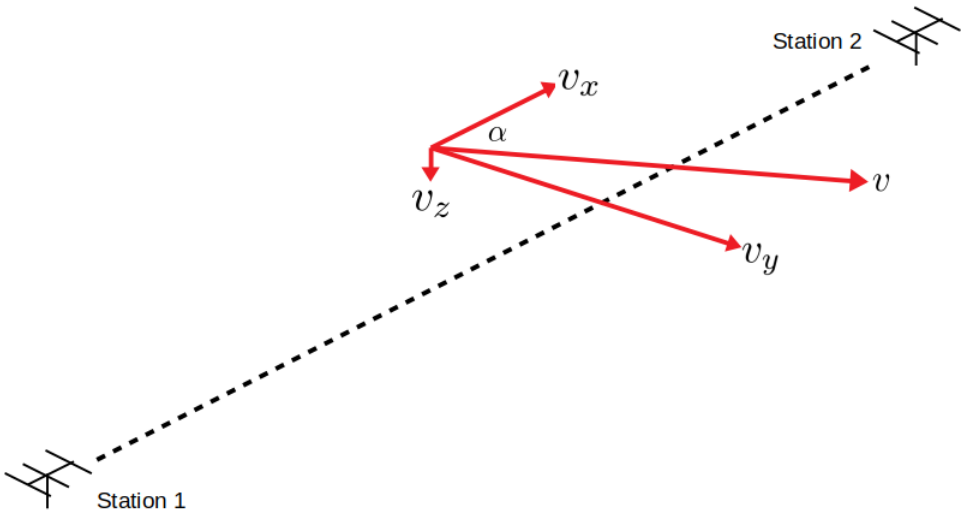

Figure 1: A meteor with velocity v has 3 components: v_x, v_y, v_z in the reference frame of the the two stations. α is the angle between the meteor direction and the direct (longitudinal) path separating the stations (dashed line). v_z is assumed to be negligibly small compared to the velocity components in the horizontal plane.

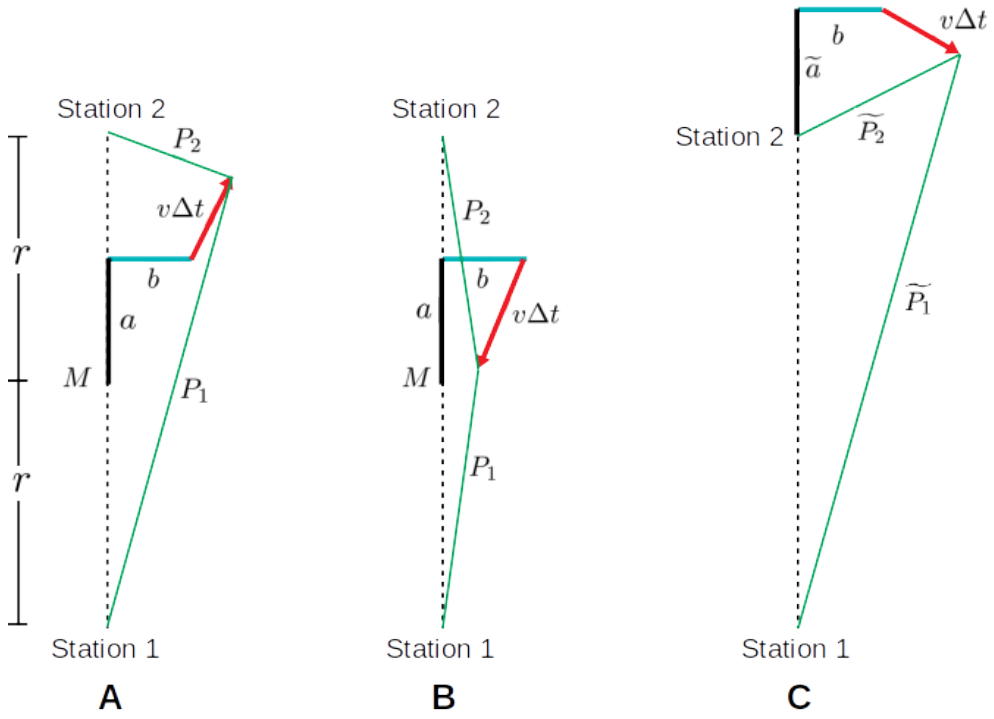

Figure 2: Top view of trajectories that affect the magnitude and sign of the Doppler shift. A meteor ping traveling a distance $v\Delta t$ appears at an offset $\sqrt{a^2+b^2}$ from the midpoint M between two stations separated by a distance $2r$. A and B are forward scattering geometries. C illustrates backward scattering with position vectors $\widetilde{P_1}$ and $\widetilde{P_2}$.

Manning considered meteors located at the midpoint between a transmitting and receiving station. This approach is generalized here to account for meteors appearing anywhere in the field of view of the station

antennas. Figure 2 is a top view of two stations separated by a terrestrial distance $2r$. A meteor ping of duration Δt and length $v\Delta t$ appears at a distance $\sqrt{a^2+b^2}$ from the midpoint M, where a and b represent the longitudinal and transverse components of the offset, respectively. The orientation of v_x and v_y with respect to the fixed stations will determine the Doppler shift. In Figure 2A, a signal propagating from Station 1 to the meteor head along path P_1 experiences a negative frequency shift. The path P_2 reflecting from the meteor to Station 2, on the other hand, imposes a positive shift. These shifts tend to cancel. The transverse component v_y moves the meteor head away from both stations resulting in a negative chirp. The situation is reversed in Figure 2B, where P_1 causes up-chirp and P_2 is down-chirped as the signal propagates from Station 1 to Station 2. The transverse velocity produces a net positive Doppler shift. When the meteor crosses the DX direct path (dashed vertical lines in Figure 2), the Doppler shift on a ping will be both positive and negative.

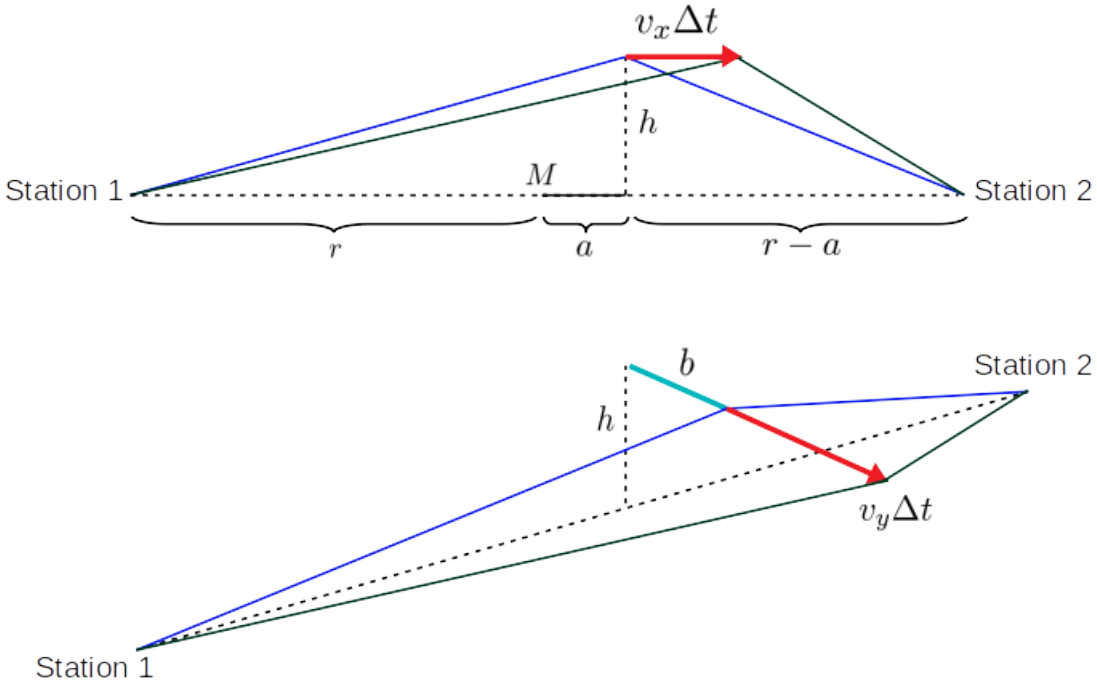

Figure 3: Geometry for calculating the forward-scattering propagation paths. Top: Meteor head with velocity v_x in the longitudinal direction as observed from the side. Bottom: Visualization of the transverse component of velocity v_y with same perspective as in Fig. 1.

The geometry of the radio wave propagation path is analyzed using Figure 3. Ignoring the curvature of the earth, the stations are separated by a terrestrial distance $2r$ with midpoint M. The top figure is from the perspective of a side observer with the transverse component obscured. A fast-moving, reflective meteor head appears between the stations at height h and longitudinal midpoint offset a. It travels a distance $v_x\Delta t$ to define a new path (green line). Note that the longitudinal velocity v_x is negative for α in the range $90-270°$. The bottom figure helps visualize the transverse path in which the meteor head travels a distance $v_y\Delta t$ that adds to or subtracts from the offset segment b, again depending on α. The time-dependent propagation path from Station 1 to the meteor head is:

$$P_1(t) = \sqrt{h^2 + (r + a + v_x t)^2 + (b + v_y t)^2} \tag{1}$$

and from the meteor head to Station 2:

$$P_2(t) = \sqrt{h^2 + (r - a - v_x t)^2 + (b + v_y t)^2} \tag{2}$$

where t runs from 0 to Δt. Differentiating Eqs. (1) and (2) yields the time-dependent path length changes:

$$\frac{d}{dt}P_1(t) = \frac{v\cos\alpha(r + a + vt\cos\alpha) + v\sin\alpha(b + vt\sin\alpha)}{\sqrt{h^2 + (r + a + vt\cos\alpha)^2 + (b + vt\sin\alpha)^2}} \tag{3}$$

$$\frac{d}{dt}P_2(t) = \frac{-v\cos\alpha(r - a - vt\cos\alpha) + v\sin\alpha(b + vt\sin\alpha)}{\sqrt{h^2 + (r - a - vt\cos\alpha)^2 + (b + vt\sin\alpha)^2}} \tag{4}$$

where v_x and v_y are written in terms of v and α. The classical Doppler shift for forward scattering is [4]:

$$\Delta f_F = \pm\frac{1}{\lambda}\left[\frac{d}{dt}P_1(t) + \frac{d}{dt}P_2(t)\right] \tag{5}$$

where λ is the radio wavelength. The meteors are assumed to be traveling much slower than the speed of light.

Setting $h = b = \alpha = 0$ places the meteor directly on the longitudinal path between the two stations. This makes $\Delta f_F = 0$, as expected. Setting $\alpha = 90°$ and $a = b = 0$ recovers Manning's result. For the forward scattering geometry, Manning assumes meteor paths that are close to the midpoint M, which allows longitudinal path length changes to be neglected compared to transverse. In practice, forward scattering takes place in a broad region defined by the overlapping antenna radiation patterns.

Backward Scattering. In the back-scattering geometry, the meteor ping appears *outside* the space between the two stations. This is sketched in Figure 2C, where $\widetilde{P_1}$ and $\widetilde{P_2}$ both produce up-chirp in the longitudinal direction and down-chirp in the transverse direction. Note that $\widetilde{a}$ is the x-component of the position vector that locates the start of the meteor burn relative to Station 2; the initial position vector $\widetilde{P_2}$ has magnitude $\sqrt{h^2 + \widetilde{a}^2 + b^2}$. As before, the Doppler shift observed at the stations will depend on the magnitude and orientation of the vector $v\Delta t$.

The time-dependent path length changes are found following the same procedure as used for forward-scattering:

$$\frac{d}{dt}\widetilde{P_1}(t) = \frac{v\cos\alpha(\widetilde{a} + 2r + vt\cos\alpha) + v\sin\alpha(b + vt\sin\alpha)}{\sqrt{h^2 + (\widetilde{a} + 2r + vt\cos\alpha)^2 + (b + vt\sin\alpha)^2}} \tag{6}$$

$$\frac{d}{dt}\widetilde{P_2}(t) = \frac{v\cos\alpha(\widetilde{a} + vt\cos\alpha) + v\sin\alpha(b + vt\sin\alpha)}{\sqrt{h^2 + (\widetilde{a} + vt\cos\alpha)^2 + (b + vt\sin\alpha)^2}} \tag{7}$$

Eqs. (6) and (7) are summed to produce the Doppler shift from head echoes in backward-scattering:

$$\Delta f_B = \pm\frac{1}{\lambda}\left[\frac{d}{dt}\widetilde{P_1}(t) + \frac{d}{dt}\widetilde{P_2}(t)\right] \tag{8}$$

The collinear Doppler radar arrangement is obtained by setting $h = b = \alpha = 0$. Eq. (8) generates the expected maximum frequency shift of $\Delta f_B = \pm 2v/\lambda$ [5].

Model Results. To investigate forward scattering, the radio frequency is set to $f = c/\lambda = 222$ MHz ($c = 3 \times 10^5$ km/s). The Doppler shift scales in direct proportion to frequency, so numbers for the 50 and 144 MHz bands are found by multiplying by 0.225 and 0.65, respectively. Stations are separated by $2r = 1500$ km, the height of the meteor is taken to be $h = 90$ km, the ping duration is set to $\Delta t = 100$ ms, and the head velocity $v = 40$ km/s. Changing any of these parameters will affect the Doppler shift, although direct scaling is not possible in the model.

We can calculate the initial Doppler shift as well as any frequency chirp that occurs over the duration of the 100 ms ping. Figure 4A is for a ping that originates at the midpoint with only a longitudinal component of velocity ($v_x = 40$ km/s; $v_y = 0$). The absolute frequency shift is < 5 Hz. When the ping appears at a distance $a = 150$ km down-range from the midpoint, the initial Doppler shift is offset by -180 Hz again with minimal chirp (Fig. 4B).

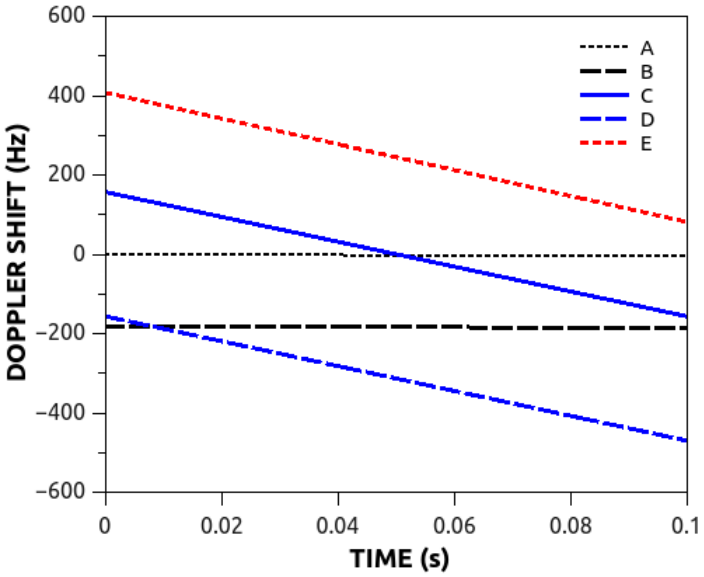

Figure 4: Calculated forward-scatter Doppler shift over the duration of a 100 ms ping at 222 MHz. Meteor head velocity 40 km/s, station separation 1500 km. A) $a = b = \alpha = 0$. The ping originates at the midpoint and travels in a direct line to Station 2. B) Same as A except the ping appears 150 km down-range from midpoint. C) Meteor head with only transverse velocity; $\alpha = 90°$, $a = 0$, $b = -2$ km. D) Same as C except $b = +2$ km. E) Meteor head with equal longitudinal and transverse velocities; $\alpha = 45°$, $a = 150$ km, $b = -5$ km.

Figure 4C depicts a ping with trajectory that perfectly straddles the midpoint ($a = 0$) with only a transverse velocity ($v_x = 0$; $v_y = 40$ km/s; $\alpha = 90°$). The 4 km path spans the range $b = \pm 2$ km. The Doppler shift decreases from a maximum of $+157$ Hz, goes to zero as the head passes through the midpoint, and then reaches the final down-chirp of -157 Hz at $t = 100$ ms. In Figure 4D, the ping appears at $b = +2$ km and travels 4 km in the transverse direction. There is an initial Doppler offset of -157 Hz with down-chirp that pushes the frequency shift to -470 Hz. A generic ping is shown in Figure 4E. The longitudinal and transverse components of velocity are the same ($v_x = 28.3$ km/s; $v_y = 28.3$ km/s; $\alpha = 45°$), with range offsets $a = 150$ km and $b = -5$ km. An initial Doppler shift and subsequent down-chirp are evident.

The initial Doppler shift (i.e. at $t = 0$) is a strong function of the vector that defines the meteor path. Figure 5 shows calculated initial frequency shifts with $h = 90$ km, station separation 1500 km, and radio frequency 222 MHz. The angle α is the relative orientation of the velocity vector to the DX path and spans the range $0 - 360°$. The curve of Fig. 5A is for range offsets $a = 150$ km and $b = 20$ km, and head

velocity $v = 40$ km/s. When the transverse offset is placed on the other side of the DX path ($b = -20$ km) the curve in Fig. 5B is generated, which is the negative of Fig. 5A. Fig. 5C is for the same conditions as Fig. 5A except the head velocity is reduced to 15 km/s. The curves show a pronounced initial Doppler shift when the meteor is moving primarily in the transverse direction.

We have seen that the Doppler shift may change over the duration of a ping, i.e. there can be distinct down-chirp. Figure 5D is the calculated frequency shift at the *end* of a 100 ms ping for the same conditions as A. In addition to an initial Doppler shift, the spectrum of the ping is broadened by as much as 400 Hz for meteor heads with dominant transverse trajectories ($v_y \gg v_x$).

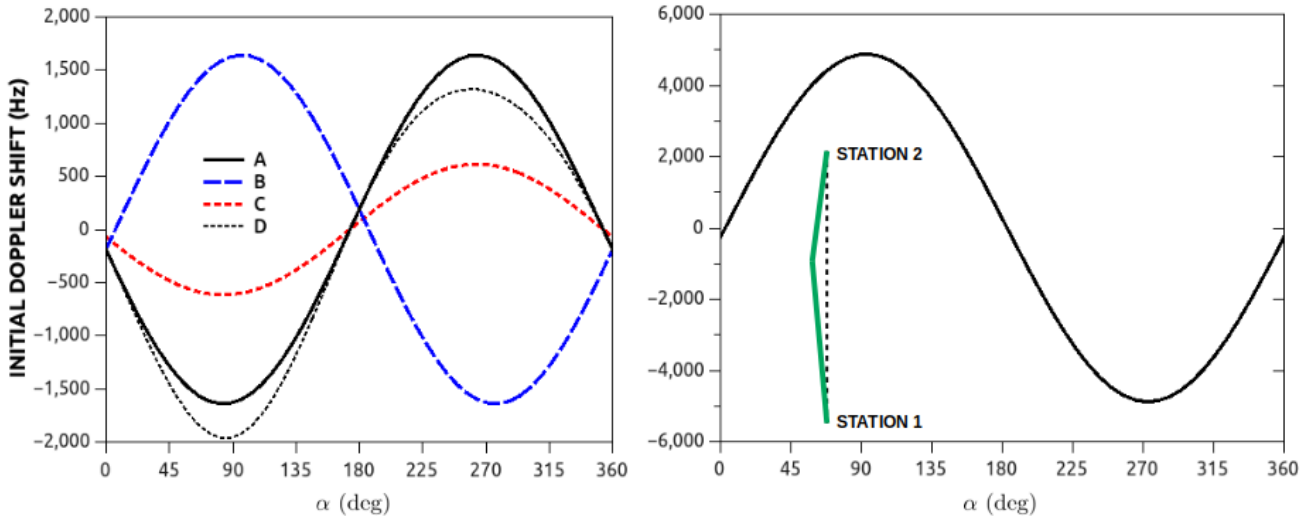

Figure 5: Analysis of the initial forward-scatter Doppler shift for different meteor head velocity vectors. Station separation is 1500 km and radio frequency is 222 MHz. Left: A) The meteor appears at range offsets $a = 150$ km and $b = 20$ km from the midpoint M. The velocity magnitude is set at 40 km/s and the angle α is varied over 360°. B) Same as A except $b = -20$ km. C) Same as A except $v = 15$ km/s. D) Same as A except $t = 100$ ms showing the effect of down-chirp over the duration of a ping. Right: Calculated initial Doppler shift for meteor with $v = 40$ km/s appearing at $\sim 5°$ in the field of view. Note the larger y-axis scale. The inset is a sketch of the path for range offsets $a = 150$ km, $b = -60$ km, and $2r = 1500$ km.

The calculations in Figs. 5 A-D are for meteors very close to the station separation midpoint. The radiation pattern of an antenna allows pings to be detected over a considerably wider range. For example, an antenna radiation lobe extending ±5° will capture pings with $b = \pm 60$ km tangential range offsets. Figure 5 (right) shows that the initial Doppler shift increases considerably when $b = -60$ km; other parameters are identical to B. The path is sketched in the inset.

Meteor back-scatter has been shown to be effective for VHF communication over path lengths that are too long for tropo-scatter but too close for forward reflections from the E-layer. To the author's knowledge, this has only been effective on the 50 MHz amateur band. Antenna elevation may allow for forward scattering on shorter DX paths, but this capability is uncommon on frequencies below 144 MHz. Referring to Figure 2C, pings appear in relatively close proximity to Station 2. Narrow antenna radiation patterns are a disadvantage here, as a wider view of the sky increases the probability of ping detection.

To assess the backward-scatter Doppler shift, the frequency is taken as 50 MHz, the ping occurs at a height $h = 90$ km with head velocity $v = 20$ km/s. The stations are separated by a distance of 1000 km, which is representative of a realistic back-scatter DX path.

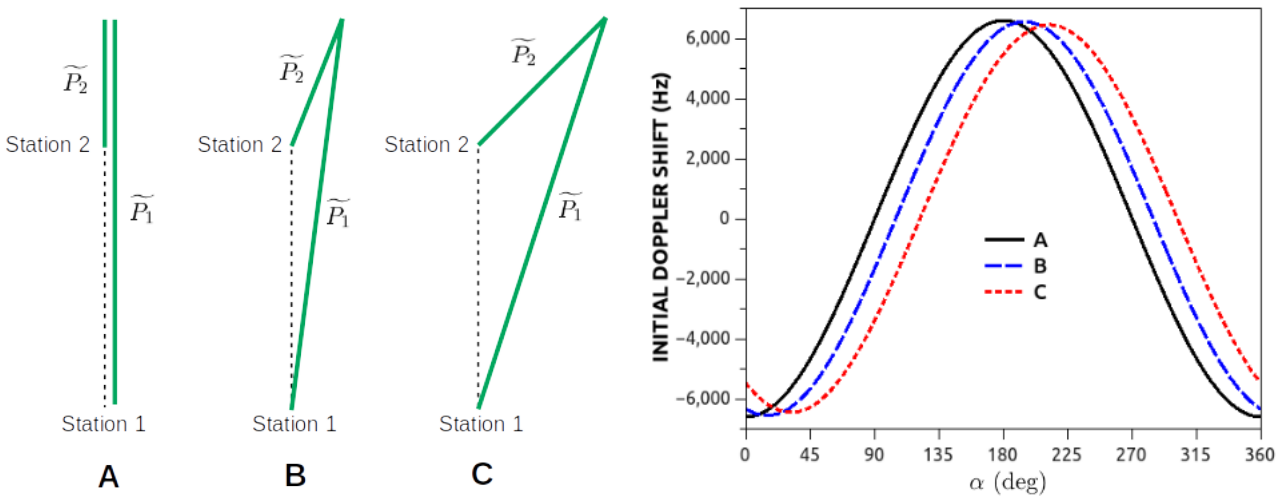

Figure 6: Calculated back-scatter Doppler shift for meteor head echoes for three different range geometries defined by $\widetilde{a}$ and b as shown in Fig. 2C. A) $\widetilde{a} = 500$ km and $b = 0$ km; B) $\widetilde{a} = 500$ km and $b = 200$ km; C) $\widetilde{a} = 500$ km and $b = 500$ km. Radio frequency is 50 MHz, station separation $2r = 1000$ km, head velocity $v = 20$ km/s, and $h = 90$ km.

Calculations are presented in Figure 6 for three illustrative cases sketched at left: A) down-range distance from Station 2 of $\widetilde{a} = 500$ km and $b = 0$ km; B) $\widetilde{a} = 500$ km and $b = 200$ km; C) $\widetilde{a} = 500$ km and $b = 500$ km. As before, α is the angle between the velocity vector and a line tangent to the DX path. Doppler shifts approach the back-scatter limit of $2v/\lambda = \pm 6.67$ kHz when there is a strong longitudinal component of velocity ($v_x \gg v_y$).

Digital Modes. FSK441 is a high-speed digital communication protocol for meteor scatter communication that was introduced by Joe Taylor in 2001 [6]. It uses four-tone frequency shift keying to convey messages at 441 baud corresponding to 147 alpha-numeric characters per second. Message length depends on character count. For example, a message sent to a DX station with a 2x3 callsign from a 2x3 callsign station with a four-digit grid locator report occupies 129 ms. There is no forward error correction, but partial decoding of messages is possible.

FSK441 provides compensation for VFO offset, initial Doppler shift, and chirp on the ping. This is performed in the frequency domain by the *FORTRAN* subroutines mtdecode.f90 and longx.f90. When a potential ping is located in the received audio stream, a fast Fourier transform generates its power spectrum. The decoder will attempt to locate spectral peaks at the positions of the four tones that are separated by 441 Hz. The frequency resolution is 43 Hz, which defines the step-size of the search. FSK441 can search the power spectrum over an operator-defined range as large as ±600 Hz. The difference frequency between transmitter and receiver is identified when the energy of the digitally filtered power spectrum is maximum.

A hard frequency offset arises from a combination of VFO mismatch and initial Doppler shift. To accommodate Doppler-induced broadening of the peaks due to chirp on the ping, digital band-pass filtering is implemented in the software. Peaks having width $\sim$ 100 Hz are placed at the anticipated positions of the four tones (see Fig. 7). In the automatic detection mode of the multi-tone decoder, the ping can have duration ranging from 40 ms to 1 second. Frequency chirp $>$ 100 Hz will cause the peaks to wash out. Longer pings, higher radio frequencies, and fast meteors moving primarily in the transverse direction (forward scattering) or longitudinal direction (backward scattering) contribute to this chirp and reduce the likelihood of obtaining message decodes.

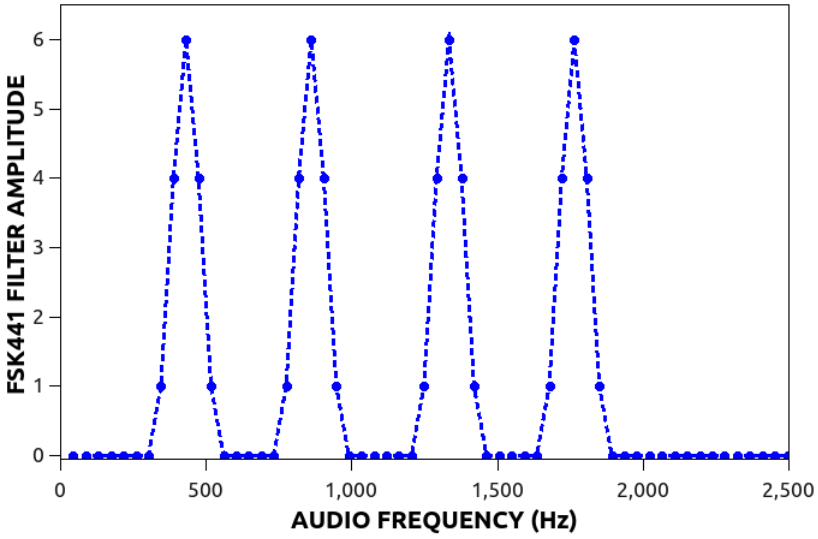

Figure 7: Digital filter used to locate the difference frequency of a multi-tone ping in FSK441. The filter is moved incrementally through the power spectrum of the ping in discrete steps of 43 Hz. The difference frequency between signal and reference frames is found when the filtered energy is maximum. The band-pass filters are separated by the approximate baud rate of 441 Hz with bandwidth $\sim$ 100 Hz. The plot shows the filters centered at 430, 860, 1333, and 1763 Hz corresponding to possible positions of the four tones in the audio spectrum.

The MSK144 protocol was developed in 2017 to make use of faster computer hardware than was available in 2001 [7]. Offset quadrature phase-shift keying results in baud and character rates that are 4.53 and 1.7 times higher than FSK441, respectively. Messages are sent repeatedly in 72 ms frames that include forward-error correction, cyclical redundancy check, and two 4 ms, 8-bit synchronization words. Frame averaging dramatically increases sensitivity and decode reliability.

The 8-bit synchronization word 0,1,1,1,0,0,1,0 as rendered by MSK144 is shown in Figure 8 (left). There are two concurrent waveforms $I(t)$ and $Q(t)$ corresponding to in-phase and quadrature components, respectively. Bits 0 and 1 are generated when the waveforms reach -1 and 1, respectively. Note that the I and Q are phase-shifted 90° so that one component is 0 when the other is ± 1. Bits are separated by 500 μs corresponding to a baud rate of 2000 bits/s. The two 4 ms sync waveforms start at $t = 0$ and at $t = 28$ ms of the 72 ms frame.

The transmitted audio signal must be an entirely real waveform. The in-phase and quadrature components are combined to produce the waveform $I(t)\cos 2\pi f_c t - Q(t)\sin 2\pi f_c t$, where the center frequency $f_c = 1500$ Hz [7]. The audio waveform for the 8-bit synchronization word is shown in Figure 8 (right). Modulation at 1500 $\pm$ 500 Hz is evident. The audio sampling rate is 12000 samples/s.

We are interested in pings with duration $\sim$ 100 ms as might be encountered with forward scattering on the 222 MHz band. MSK144 implements a short-pulse decoder for this purpose. Insight into its operation can be obtained by examining *FORTRAN* subroutines mskrtd.f90, msk144spd.f90, msk144sync.f90, and msk144_freq_search.f90. The audio data stream (typically 15 s) is analyzed in near real-time by selecting sequential 0.597 s time blocks, interleaved by 0.2985 s so there is no possibility of data loss. An FFT followed by an inverse FFT produces a 0.597 s complex time waveform with in-phase and quadrature components, similar to Fig. 8 (left). The first 0.558 s of the this waveform is partitioned into 28 partially overlapping frames of duration 72 ms. The overlap is 18 ms, corresponding to 1/4 frame.

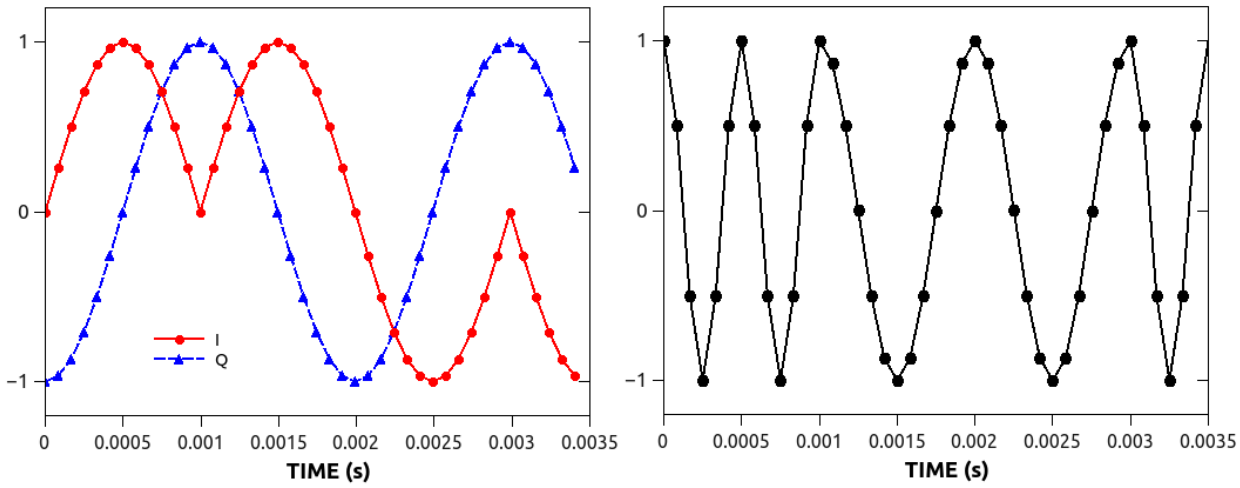

Figure 8: MSK144 8-bit synchronization word. Left: In-phase (I) and quadrature (Q) components render the digital sequence: 0,1,1,1,0,0,1,0 where bit 1 is produced when either waveform reaches 1 and bit 0 corresponds to waveform amplitude -1. Right: Transmitted audio signal obtained by combining $I(t)$ and $Q(t)$ with center frequency 1500 Hz. Two modulation periods at 0.0005 and 0.001 s can be distinguished, corresponding to tones of 2000 and 1000 Hz, respectively. Time step is the inverse of the audio sampling rate: $[12000\ \text{Samples/s}]^{-1} = 83\ \mu\text{s}$.

A coarse frequency search is performed on each of the 28 frames by generating their squared signal spectrum. The squaring operation places the modulation peaks at 2000 and 4000 Hz. If the operator sets the frequency tolerance for 200 Hz, any frame displaying a peak inside the limits 2000 ± 400 Hz or 4000 ± 400 Hz is tagged as a candidate for further time and frequency synchronization. If the initial search produces fewer than three candidate frames, a second search is implemented having greater sensitivity but maintaining the same frequency tolerance.

After all possible candidates are identified, they are sliced from the main 0.597 s waveform as a 0.216 s time block corresponding to three sequential 72 ms frames, indexed j = 1,2,3. Time synchronization has not yet been established, but the frequency offset between transmitter and receiver is known to ±13.89 Hz. Fine synchronization is obtained by cross-correlating data in the 3-frame candidate block with the reference waveform R displayed in Fig. 8 (left). This is an iterative process in which the frequency of the signal is adjusted in each of the three frames over a range ±200 Hz in 2 Hz increments. Corresponding elements in the three frames are then summed to produce an average signal frame with $k = 864$ elements:

$$S_k = \sum_{j=1}^{3} (I_{j,k} + iQ_{j,k}) \tag{9}$$

where $i = \sqrt{-1}$. Cross-correlation is accomplished by taking the dot product of the averaged signal S with the reference synchronization waveform R:

$$X_m = \sum_{k=1}^{42} S^*_{k+m} R_k + \sum_{k=337}^{378} S^*_{k+m} R_k \tag{10}$$

where * indicates the complex conjugate of S. The 8-bit sync word occupies 42 time slots so it is only necessary to carry out this operation at its two expected locations as shown in Eq. (10). X_m is calculated

for $m = 864$ different time offsets between S and R. Temporal precision is the inverse of the audio sampling rate: 83 μs. There are 200 frequency increments and 864 time increments resulting in 172,800 correlations for each candidate. The final time and frequency offsets between signal and reference are identified when the correlation amplitude $|X_m|$ is maximum.

Discussion. FSK441 and MSK144 have limited ability to compensate for VFO offsets and Doppler shifts. FSK441 can accommodate as much as ±600 Hz compared to ±200 Hz for MSK144. If chirp exceeds 100 Hz *during* a ping the FSK441 decoder may not properly synchronize. MSK144 uses a combination of spectral and coherent time-domain signal processing to correct for chirp as large as 200 Hz in each 72 ms time block that comprises a ping.

Our analysis of forward scattering from fast moving meteor heads at 222 MHz indicate that – as a general conclusion – the Doppler shifts are too large to allow decoding with either FSK441 or MSK144. Consider the calculation shown in Fig. 5 (right). Meteor heads can have trajectories with any angle α in the range $0 - 360°$, but only about 1% have a possibility of being decoded. Doppler shifts within the FSK441 frequency tolerance of ±600 Hz will exist if the following conditions are satisfied: head velocities < 15 km/s, meteor burns very close to the midpoint, and negligible VFO misalignment (Fig. 5C). High levels of ionization are needed at UHF, however, suggesting that meteors with low velocities are unlikely to produce useful pings.

Meteor scatter QSOs are routinely made using both modes on the 222 MHz band. It would appear that these pings are reflections from the quasi-stationary meteor trail, *not* the head. Doppler shift from the meteor trails has been attributed to ionized particle diffusion and the presence of wind in the E-layer. These result in much smaller frequency shifts than induced by the velocity of the head [8].

The calculated Doppler shift from head echoes in a back-scatter arrangement at 50 MHz is shown in Fig. 6. The frequency shifts are multiple kHz, which is far outside the ability of either FSK441 or MSK144 to compensate. In this situation, it is nearly certain that reflections are entirely from trails.

As a final comment, it is important to point out that the MSK144 decoder operates in the time-domain with signals having recognizable phase. Loss of coherence will, therefore, impact decoder sensitivity. Group delay in the receiver passband can contribute significantly to phase distortion. This may be an issue with transverters that are routinely used on the 222 MHz band. The program developers have described a straightforward procedure for phase equalization, customized for an operator's specific hardware [7].

Conclusion. A general model for forward- and backward-scattering from meteor head echoes reveals very large Doppler shifts. Important parameters include the head velocity vector, path geometry, and radio frequency. The FSK441 and MSK144 decoders generally cannot correct for Doppler shifts originating from a fast moving meteor head. These digital modes, however, have proven to be highly effective for meteor scatter communications in a wide variety of conditions, suggesting that pings originate primarily from the relatively stationary trail, not the head.

References

[1] W. Bain, "VHF Propagation by Meteor Trail Ionization", QST (May 1974).

[2] S. Close, M. Oppenheim, S. Hunt, and L. Dyrud, "Scattering characteristics of high-resolution meteor head echoes detected at multiple frequencies", J. Geophys. Res. **107** (2002).

[3] L.A. Manning, "The Theory of the Radio Detection of Meteors", J. Appl. Phys. **19** 689 (1948).

[4] J. Richardson and W. Kuneth, "Revisiting the Radio Doppler Effect from Forward-scatter Meteor Head Echoes", WGN **26** 117 (1998).

[5] Setting setting $a = r$ in Eq. (5) and $\widetilde{a} = 0$ in Eq. (8) creates limit cases that connect the backward- and forward-scatter models. This yields $\Delta f_R = \Delta f_B$ and demonstrates the internal consistency of the analysis.

[6] J. Taylor, "WSJT: New Software for Meteor Scatter Communication", QST (Dec. 2001).

[7] S. Franke and J. Taylor, "The MSK144 Protocol for Meteor Scatter Communication", QEX (Sep/Oct. 2017).

[8] G.R. Sugar, "Radio Propagation by Reflection from Meteor Trails", Proc. IEEE **52** 116 (1964).

Updates to this document will be posted at: www.sportscliche.com/wb2fko/tech.html.